View metadata, citation and similar papers at core.ac.uk
brought to you by CORE
provided by Elsevier - Publisher Connector

Cell Metabolism
Article

TRPM Channels Mediate Zinc Homeostasis and Cellular Growth during *Drosophila* Larval Development

Plamen Georgiev,[1,5] Hanneke Okkenhaug,[1] Anna Drews,[2] David Wright,[3] Sachar Lambert,[2] Melanie Flick,[2] Valentina Carta,[1] Cecile Martel,[1] Johannes Oberwinkler,[2] and Padinjat Raghu[1,4,*]
[1]Inositide Laboratory, Babraham Institute, Babraham Research Campus, Cambridge CB22 3AT, UK
[2]Emmy Noether Research Group, Experimentelle und Klinische Pharmakologie und Toxikologie, Uniklinikum des Saarlandes, 66421 Homburg, Germany
[3]Department of Physiology, Development, and Neuroscience, University of Cambridge, Cambridge CB2 3AT, UK
[4]Present address: National Centre for Biological Sciences, Bellary Road, Bangalore 560065, India
[5]Present address: Max-Planck Institute of Immunobiology, Stübeweg 51, D-79108 Freiburg, Germany
*Correspondence: praghu@ncbs.res.in
DOI 10.1016/j.cmet.2010.08.012

SUMMARY

TRPM channels have emerged as key mediators of diverse physiological functions. However, the ionic permeability relevant to physiological function in vivo remains unclear for most members. We report that the single *Drosophila* TRPM gene (*dTRPM*) generates a conductance permeable to divalent cations, especially Zn^{2+} and in vivo a loss-of-function mutation in *dTRPM* disrupts intracellular Zn^{2+} homeostasis. TRPM deficiency leads to profound reduction in larval growth resulting from a decrease in cell size and associated defects in mitochondrial structure and function. These phenotypes are cell-autonomous and can be recapitulated in wild-type animals by Zn^{2+} depletion. Both the cell size and mitochondrial defect can be rescued by extracellular Zn^{2+} supplementation. Thus our results implicate TRPM channels in the regulation of cellular Zn^{2+} in vivo. We propose that regulation of Zn^{2+} homeostasis through dTRPM channels is required to support molecular processes that mediate class I PI3K-regulated cell growth.

INTRODUCTION

Transient receptor potential (TRP) proteins are a large family of cation channels with a range of ionic permeabilities and functions (Ramsey et al., 2006). Although many TRP channels appear to mediate sensory transduction in eukaryotes (Damann et al., 2008), it is increasingly clear that some members of this family are also involved in regulating fundamental cellular processes unrelated to sensory transduction.

TRP channels have been classified into several subfamilies. Of these, the TRPM subfamily is distinguished by the presence of a unique TRPM domain at the N terminus. Genes encoding TRPM-like channels are not found in the yeast genome but are found in a range of metazoan species including *C. elegans*, *Drosophila*, zebrafish, and mammals (Padinjat and Andrews, 2004). Four TRPM genes have been described in *C. elegans* (Xiao and Xu, 2009). Of these, *gon-2* and *gtl-1* have been implicated in intestinal electrolyte homeostasis, postembryonic mitosis in the gonad, and body wall contraction (Kwan et al., 2008; Teramoto et al., 2005; West et al., 2001). The zebrafish genome encodes four TRPM genes; a mutant in *trpm7* shows defects in skeletogenesis, embryonic melanophore formation, growth, and touch responses (Elizondo et al., 2005). Mammalian TRPM channels have been linked to key physiological processes such as pancreatic β cell function (Wagner et al., 2008), magnesium homeostasis (Schlingmann et al., 2002), cell viability (Schmitz et al., 2003), anoxic cell death (Aarts et al., 2003), cold sensation (McKemy et al., 2002; Peier et al., 2002), and taste transduction (Zhang et al., 2003).

A range of ionic permeabilities has been reported for TRPM channels (reviewed in [Fleig and Penner, 2004; Owsianik et al., 2006]). Four members, TRPM2 (Xia et al., 2008), TRPM3α2 (Oberwinkler et al., 2005), TRPM6 (Voets et al., 2004), and TRPM7 (Nadler et al., 2001), are reported to be permeable to Mg^{2+}. Loss-of-function phenotypes in TRPM7 are reported to be rescued by Mg^{2+} supplementation (Sahni and Scharenberg, 2008; Schmitz et al., 2003), and supplementation with Ca^{2+} and Mg^{2+} has been reported to rescue distinct aspects of the zebrafish *trpm7* mutant phenotype (Elizondo et al., 2005). However, a recent study reported no defects in acute Mg^{2+} uptake or total cellular Mg^{2+} in lymphoctyes from murine TRPM7 KO animals (Jin et al., 2008). Thus, presently the ionic permeability relevant to the cellular function of TRPM7 in vivo remains unresolved.

The *Drosophila* genome is reported to encode a single TRPM gene (*dTRPM*) and thus offers a unique opportunity to define the properties and functional requirement of TRPM channels in a metazoan model. In this study, we report the expression and functional characterization of *dTRPM* along with the analysis of a *dTRPM* null mutant. Our results define a role for dTRPM channels in regulating Zn^{2+} homeostasis and cell size during *Drosophila* development.

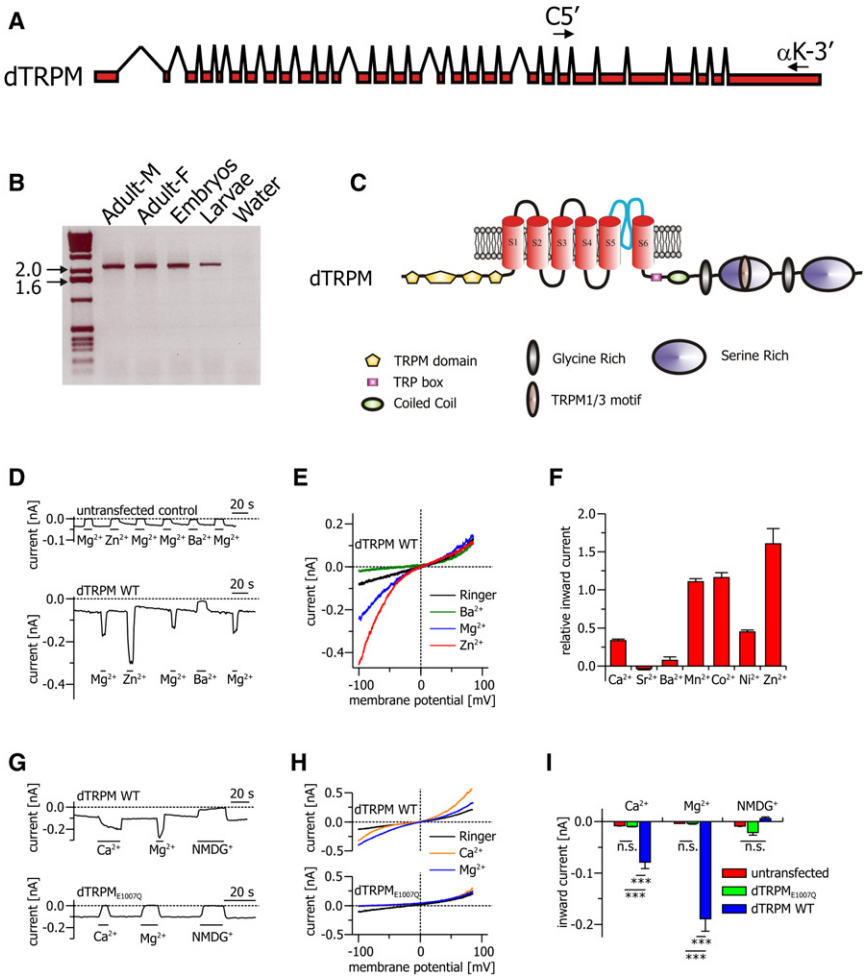

Figure 1. Gene Structure and Functional Expression of *dTRPM*

(A–C) (A) The intron-exon structure of the *dTRPM* gene. Exons are shown in red, and their position on the gene sequence is derived from the sequencing of the cDNA cloned during this study. The positions of primers C5′ and αK-3′ used in the RT-PCR analysis in (B) are marked. (B) PCR analysis of cDNA generated from multiple *Drosophila* stages. Primers C5′ and αK-3′ generate a single 2.3 kb PCR product showing expression of this cDNA at all stages. (C) Depiction of the protein encoded by the *dTRPM* cDNA cloned during this study. Putative transmembrane domains S1–S6 are marked, and the location of other domains is indicated on the panel.

(D–F) Divalent cation permeable channels are formed in the plasma membrane by dTRPM proteins. (D) Amplitudes of inward (−80 mV) currents measured during solution exchanges that replaced all extracellular cations with the indicated divalent cation (10 mM). In untransfected HEK293 cells (upper panel), this reduced the inward currents to very low levels. In cells transfected with *dTRPM* (lower panel), sizable inward currents were measured when only divalent cations were present extracellularly. (E) Current-voltage relationships were measured in a dTRPM-expressing cell with voltage ramps during the recording shown in (D) (lower panel). (F) Absolute inward currents (measured as shown in D) were leak subtracted (leak current was estimated by replacing all cations with NMDG at the end of the recording) and normalized to the inward currents carried by Mg^{2+} measured in the same cell. This allowed the comparison of relative inward currents for the various divalent cations (all measured at 10 mM). The largest amplitudes were obtained with Zn^{2+}.

(G–I) (G) In cells transfected with *dTRPM*$_{E1007Q}$ (lower panel), the inward currents measured with divalent cations as charge carriers were absent compared to cells transfected with wild-type *dTRPM* (upper panel). (H) Current-voltage relationships were measured during the recordings shown in (G). (I) Statistical analysis of the absolute inward currents (not leak subtracted) measured during experiments performed as shown in (G) and (H). Inward currents significantly larger than in untransfected cells were measured with Ca^{2+} and Mg^{2+} as the only charge carriers in cells expressing wild-type dTRPM channels, but not in cells expressing dTRPM$_{E1007Q}$. Error bars indicate SEM.

RESULTS

A Single TRPM Gene in *Drosophila*

Although a single *Drosophila* TRPM gene has been reported (Montell, 2003; Padinjat and Andrews, 2004), the nature of the encoded gene product and functional data are currently unavailable. In the current version of the *Drosophila* genome, *dTRPM* is annotated as CG34123. We cloned a cDNA of 5847 bp from fly head RNA that included 30 exons from CG34123. RT-PCR analysis using primers C5′ and αK-3′ (Figure 1A) revealed that this transcript was expressed at all developmental stages (Figure 1B). This cDNA contains a single ORF of 5766 bp that encodes a protein of 1921 amino acids (see Figure S1 available online). When expressed in COS cells, this cDNA produced a protein of the expected relative molecular mass. The principal features of the encoded protein are shown in Figure 1C. These include an N-terminal TRPM domain, an ion channel domain; C-terminal to the sixth transmembrane domain is a TRP box, coiled-coil domain, and a long C-terminal stretch that is unusually enriched in serine and threonine residues (ca. 11%), suggesting that this domain might undergo phosphorylation, as has been demonstrated for mammalian TRPM6 (Cao et al., 2008; Clark et al., 2008) and TRPM7 (Ryazanova et al., 2004). However, unlike TRPM6/7 (Ryazanov et al., 1997), this region does not appear to encode an unconventional protein kinase (α-kinase) domain, consistent with reports (Drennan and Ryazanov, 2004) that there are no α-kinases encoded in the *Drosophila* genome. It is therefore likely that a distinct protein kinase operating in *trans* phosphorylates dTRPM. Finally, a small motif (EYTSITD) was noted in the C terminus that is highly conserved with mammalian TRPM1 and TRPM3.

dTRPM Encodes a Functional Ion Channel

When expressed in HEK293 cells, *dTRPM* induces a constitutively active conductance not seen in untransfected cells (Figures 1D and 1E). This *dTRPM*-induced conductance could be suppressed by high intracellular Mg^{2+} (Figure S2A versus Figures S2B, S2E, and S2F), a feature shared with mammalian

TRPM channels (Nadler et al., 2001; Oberwinkler et al., 2005; Voets et al., 2004). Using bi-ionic conditions, we found that the *dTRPM*-induced conductance is permeable to a wide range of divalent cations including Mg^{2+}, Ca^{2+}, Mn^{2+}, Co^{2+}, and Zn^{2+} (Figure S2H). When current amplitudes are measured for each divalent cation relative to that of Mg^{2+}, dTRPM has the highest conductivity to Zn^{2+}, followed by Mn^{2+} and Co^{2+} (Figure 1F).

We generated a pore mutant by introducing a glutamate to glutamine change at position 1007 (Figure S1), homologous to a glutamate residue in mammalian TRPM channels that has previously been shown to be critical for divalent permeability (Li et al., 2007; Mederos y Schnitzler et al., 2008; Nilius et al., 2005). When expressed in HEK293 cells, $dTRPM_{E1007Q}$ channels generated a constitutively active conductance (Figure S2C) not seen in untransfected cells (Figure S2G) that could be suppressed by applying high intracellular Mg^{2+} (Figure S2D). Importantly, $dTRPM_{E1007Q}$ channels were entirely impermeable to divalent cations, as judged by measuring current amplitudes under bi-ionic conditions (Figures 1G–1I and Figure S2F). These results clearly demonstrate that the E1007Q mutation alters the selectivity of dTRPM channels in predictable ways and therefore establish that dTRPM proteins are part of an ion-conducting pore.

dTRPM Is Required to Support Growth during Larval Development

To study the effects of dTRPM loss of function, we generated a null mutant in *dTRPM* ($dTRPM^{28}$) (Figures S3A and S3B). $dTRPM^{28}$ animals show prolonged larval development, at the end of which they arrest and die at the prepupal stage. Wild-type animals grown at 25°C spend ca. 99 hr posthatching as larvae, while the equivalent stages last ca. 135 hr in $dTRPM^{28}$ (Figure 2A). Further, $dTRPM^{28}$ larvae show a lower body weight compared to wild-type controls throughout larval development (Figure 2A), with the difference in weight being maximal ($dTRPM^{28}$ 50% lower) at the end of the second larval instar. We also evaluated the time taken to attain minimum viable weight, a key growth milestone during larval development (Mirth and Riddiford, 2007), and found that $dTRPM^{28}$ larvae take ca. 24 hr longer to achieve this relative to wild-type controls (Figure 2B). In addition, we generated animals lacking both maternal and zygotic *dTRPM* transcripts ($dTRPM^{28\Delta m\Delta z}$) (Figure S3D). By the end of the first larval instar, $dTRPM^{28\Delta m\Delta z}$ animals showed an obvious growth defect (Figure 2D), weighing less than wild-type controls. This growth defect progressed rapidly, and by the middle of the second instar $dTRPM^{28\Delta m\Delta z}$ animals were ~17% of wild-type controls (Figures 2C and 2D). $dTRPM^{28\Delta m\Delta z}$ larvae die at ca. 48 hr posthatching.

A Cell-Autonomous Requirement for *dTRPM* in Determining Cell Size in Larvae

We found that the growth defect in $dTRPM^{28}$ was underpinned by a reduction in cell size, whereas cell numbers (Figures S4F and S4G) and DNA replication (Figure S4E) were normal. For example, the circumference of $dTRPM^{28}$ salivary gland cells (Figure 2E versus Figures 2G and 2K) and fat body cells (Figure 2H versus Figures 2J and 2K) were 51% and 78% of wild-type controls, respectively. Moreover, when *dTRPM* function is reduced by transgenic RNAi ($RNAi^{TRPM}$) specifically in the salivary gland, the size of the salivary gland cells was 76% of wild-type controls (Figures 2F and 2K), leaving the size of fat body cells (where the RNAi is not induced) unaffected (Figures 2I, 2K, and 2H). These data demonstrate a cell-autonomous requirement for *dTRPM* in regulating cell size during larval growth.

Normal Activation of Class I PI3K in $dTRPM^{28}$ Salivary Gland Cells

To understand the growth phenotype of $dTRPM^{28}$, we analyzed the requirement for *dTRPM* in the context of insulin signaling. The insulin signaling pathway generates a growth-promoting signal through class I PI3K activation producing the lipid signal, phosphatidyl inositol 3,4,5 trisphosphate (PIP_3) at the plasma membrane resulting in the recruitment and phosphorylation of the PIP_3 -dependent kinase AKT/PKB (Stephens et al., 1998) to the plasma membrane. We tested class I PI3K activation in $dTRPM^{28}$ using three approaches. (1) The first is measuring PIP_3 production using a GFP-tagged PH domain specific for PIP_3 (PIP_3 probe) (Britton et al., 2002). In salivary gland cells of both feeding third instar larvae as well as white prepupae (wpp) of $dTRPM^{28}$, the level of PIP_3 probe at the plasma membrane was not reduced but in fact significantly higher than wild-type controls (Figures 3A, 3C, and 3D). Similar results were obtained from salivary gland cells of $RNAi^{TRPM}$ (Figures 3B and 3D). (2) Using phospho-specific antibodies, we found that phospho-AKT levels at the plasma membrane in $dTRPM^{28}$ salivary gland cells were higher than in controls (Figures 3E–3G), and western blot analysis showed that p-AKT levels were no different between controls and $dTRPM^{28}$ (Figure 3H). (3) Finally, western blot analysis showed that the phosphorylation of two key targets of class I PI3K signaling, S6K (Ma and Blenis, 2009) and 4E-BP, was not altered in $dTRPM^{28}$ (Figure 3H). Collectively, our results provide compelling evidence that the cell-autonomous requirement of *dTRPM* for growth occurs in the face of normal or supranormal class I PI3K activation.

dTRPM Is Required for Cell Growth Mediated by Class I PI3K and S6K Signaling

To test the requirement for *dTRPM* in class I PI3K-mediated cell growth, we overexpressed the catalytic subunit of class I PI3K in the developing larval salivary gland. In wild-type larvae, this results in a 186% increase in gland size that is principally mediated by an increase in cell size (Figure 3I versus Figures 3K and 3Q). However, in $dTRPM^{28}$ salivary glands, overexpression of the same class I PI3K transgene resulted in no significant increase in cell size (Figure 3J versus Figures 3L and 3Q). Although class I PI3K overexpression also results in a small (14%) increase in cell number, this change was indistinguishable between wild-type and $dTRPM^{28}$ glands. These data provide strong evidence that, in *Drosophila*, *dTRPM* function is required for class I PI3K-mediated cellular growth.

When overexpressed in wild-type salivary glands, *Drosophila* S6K (dS6K) causes a small increase (32%) in average cell size (Figure 3I versus Figures 3M and 3Q). By contrast, the phosphomimetic variant ($dS6K^{STDETE}$) (Barcelo and Stewart, 2002) causes a much larger (135%) increase in cell size (Figure 3I versus Figures 3O and 3Q), suggesting that in this system it is at least partially uncoupled from upstream growth control

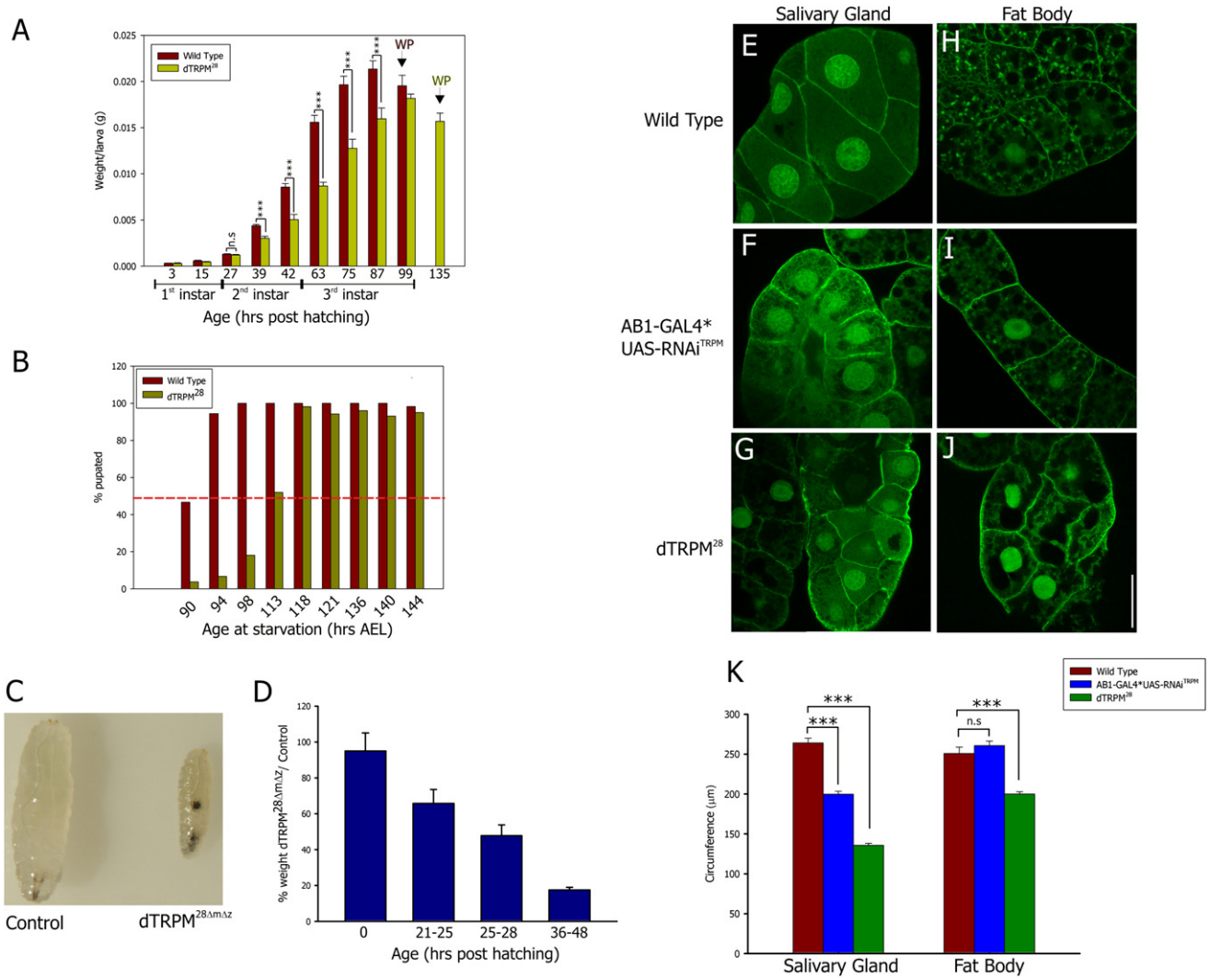

Figure 2. Growth Phenotype in *dTRPM* Mutants

(A) Growth curve comparing the weight of wild-type and *dTRPM*^{28} larvae at different developmental ages. x axis shows age in hours posthatching at 25°C. The approximate duration of each larval instar in wild-type is shown below the x axis. The weight shown for each time point is the mean ±SD (n = 100). WP indicates the time at which each genotype forms white prepupae and is coded in the same colors as the bars. Statistical significance, ***p < 0.001.

(B) A 24 hr delay in attaining minimum viable weight in *dTRPM*^{28} animals. Red dotted line denotes 50% pupariation. y axis shows the percent of animals that have pupariated. x axis shows the age (hours after egg laying, AEL) of the animals when they were transferred onto starvation medium. Statistical significance was tested using a $\chi 2$ test where statistical significance is reached when $p < 0.05$. For this data set the p value is < 0.0001.

(C) Light micrograph of a control and *dTRPM*$^{28\Delta m\Delta z}$ mid second instar larva showing the growth phenotype in the mutant.

(D) Progressive growth deficit in *dTRPM*$^{28\Delta m\Delta z}$ larvae. The weight of the *dTRPM*$^{28\Delta m\Delta z}$ animals is shown as percent of wild-type controls measured under identical conditions. x axis shows the age of animals in hrs post hatching.

(E–J) Micrographs of the salivary gland and fat body showing cell size reduction due to *dTRPM* loss of function. The plasma membrane is marked by the PIP_3 probe. Representative images of cells from the secretory part of the salivary gland in wild-type wpp (E), *dTRPM*^{28} (G); fat body cells from wild-type (H) and *dTRPM*^{28} (J) are shown. Images from salivary gland-specific knockdown of *dTRPM* by RNAi results in a size reduction only in salivary gland cells (F), while leaving the size of fat body cells unaffected (I). Scale bar for (E)–(J), 50 μm.

(K) Quantification of cell circumference in *dTRPM* mutants and wild-type controls. Cell size was assessed by measuring the circumference of cells in which the nuclei could be clearly seen. Bars are mean ±SEM (n = >30 cells from at least four animals. Statistical significance was calculated using the unpaired Student's t test (Welch's). n.s indicates $p > 0.05$; ***$p < 0.001$.

signals. We overexpressed dS6K^{STDETE} in *dTRPM*^{28} salivary glands and found that there was no significant increase in cell size (Figure 3J versus Figures 3P and 3Q). These observations strongly suggest that normal *dTRPM* function is required for cell growth subsequent to the activation of S6K.

Altered Mitochondrial Structure and Function in *dTRPM*^{28}

We performed gene expression analysis using microarrays comparing *dTRPM*$^{28\Delta m\Delta z}$ late second instar larvae with wild-type controls of the same age. The data revealed widespread

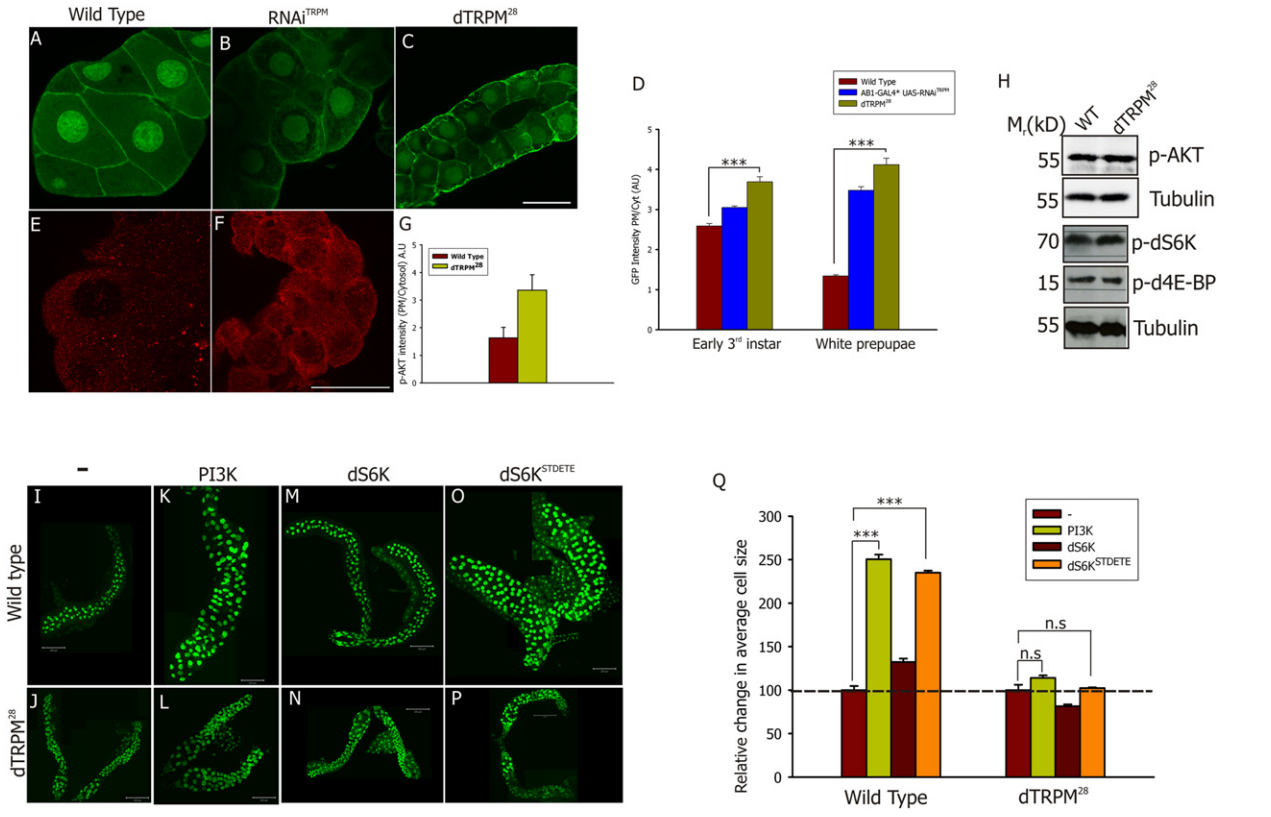

Figure 3. Class I PI3K Signaling in *dTRPM* Mutants

Micrographs of salivary glands showing the membrane localization of a GFP-tagged PIP_3 probe at the plasma membrane in wpp from wild-type (A), AB1-GAL4* UAS-RNAi^{TRPM} (B), and *dTRPM^{28}* (C). Scale bar in (A)–(C), 50 μm. (D) Y axis depicts the ratio of PIP_3 probe intensity at the plasma membrane/intensity in the cytoplasm. Data are shown from glands of both early third instar larvae and wpp. Bars are the mean ±SEM (n = >30). Statistical significance was determined using a two sample z test: n.s $p > 0.05$ (equivalent z value < 1.96); *$p < 0.05$ ($z > 1.96$), **$p < 0.01$ ($z > 2.575$), and *** for $p < 0.001$ ($z > 3.300$). Salivary glands from wpp of wild-type (E) and *dTRPM^{28}* (F) stained with an antibody to phospho-AKT. (G) Quantification of p-AKT staining on the y axis is shown as the ratio between plasma membrane and cytosolic fluorescence. Bars are the mean ±SEM (n = > 5). Scale bars in (E) and (F), 50 μm. (H) Western blots showing levels of phosphoprotein for p-AKT, p-p70S6K, and p-d4E-BP in protein extracts prepared from white prepupae of wild-type and *dTRPM^{28}*. Tubulin levels are shown as a loading control. (I–P) Maximum projection images from wild-type and *dTRPM^{28}* salivary glands overexpressing key regulators of cell growth. Wild-type (I) and *dTRPM^{28}* (J) are shown as controls. Wild-type salivary glands overexpressing class I PI3K (K) dS6K (M) and dS6K^{STDETE} (O) as well as *dTRPM^{28}* overexpressing class I PI3K (L), dS6K (N), and dS6K^{STDETE} (P) are shown. Scale bar in each panel is 200 μm. Nuclei are shown in green and have been marked using the fluorescent nuclear dye TOTO-3. (Q) Quantification of cell growth in wild-type and *dTRPM^{28}* resulting from overexpression of the cell growth regulators class I PI3K, dS6K, and dS6K^{STDETE}. The relative increase in average cell size from each genotypes is shown. The dotted line represents the cell size in wild-type and *dTRPM^{28}* without overexpression of any growth regulator. Bars represent mean ±SEM. Data represent the analysis of glands from at least four animals.

changes in gene expression involving almost 9% of genes on the array with diverse biological functions. Gene Ontology analysis revealed that among the genes downregulated in *dTRPM$^{28\Delta m\Delta z}$*, the most statistically significant category was GO3735 (structural constituent of ribosome [p = 2.58E-17]) and GO5739 (mitochondrion [p = 4.16E-35]) with both mitochondrial matrix and mitochondrial ribosomes (mitoribosomes) affected (Table S1). Of the 75 genes annotated as mitoribosomes on this array, almost all showed downregulation, although the change in transcript levels was variable. The downregulation in several mitoribosome transcripts was confirmed by real-time quantitative PCR (RT-QPCR) (Figure 4A). In sharp contrast, there was almost no downregulation of transcripts encoding components of nonmitochondrial ribosomal proteins (Table S1). These observations suggest that a selective downregulation in the levels of mitoribosomes is a major aspect of the *dTRPM* mutant phenotype.

Since mitoribosome function is required to translate proteins encoded in the mitochondrial genome (Pel and Grivell, 1994), we predicted that mitochondrial function might be altered in *dTRPM^{28}* cells. To test this, we measured ATP levels, a key output of mitochondrial function, in total larval extracts from *dTRPM^{28}*. This revealed a reduction in the levels of ATP in both *dTRPM^{28}* (Figure 4B) and *dTRPM$^{28\Delta m\Delta z}$* (data not shown) extracts. This finding demonstrates a functional consequence of altered mitochondrial function in *dTRPM^{28}*. We also imaged mitochondrial structure in salivary glands using a mitoGFP reporter. In wild-type salivary gland cells, mitochondria are visualized as individual bullet-shaped structures (Figures 4C and 4F). By contrast, in *dTRPM^{28}* salivary glands, mitochondria were fused to form long tubular structures (Figures 4E and 4H). This defect is quantified as the average volume of individual mitochondria (Figure 4I) and was cell autonomous as it was also

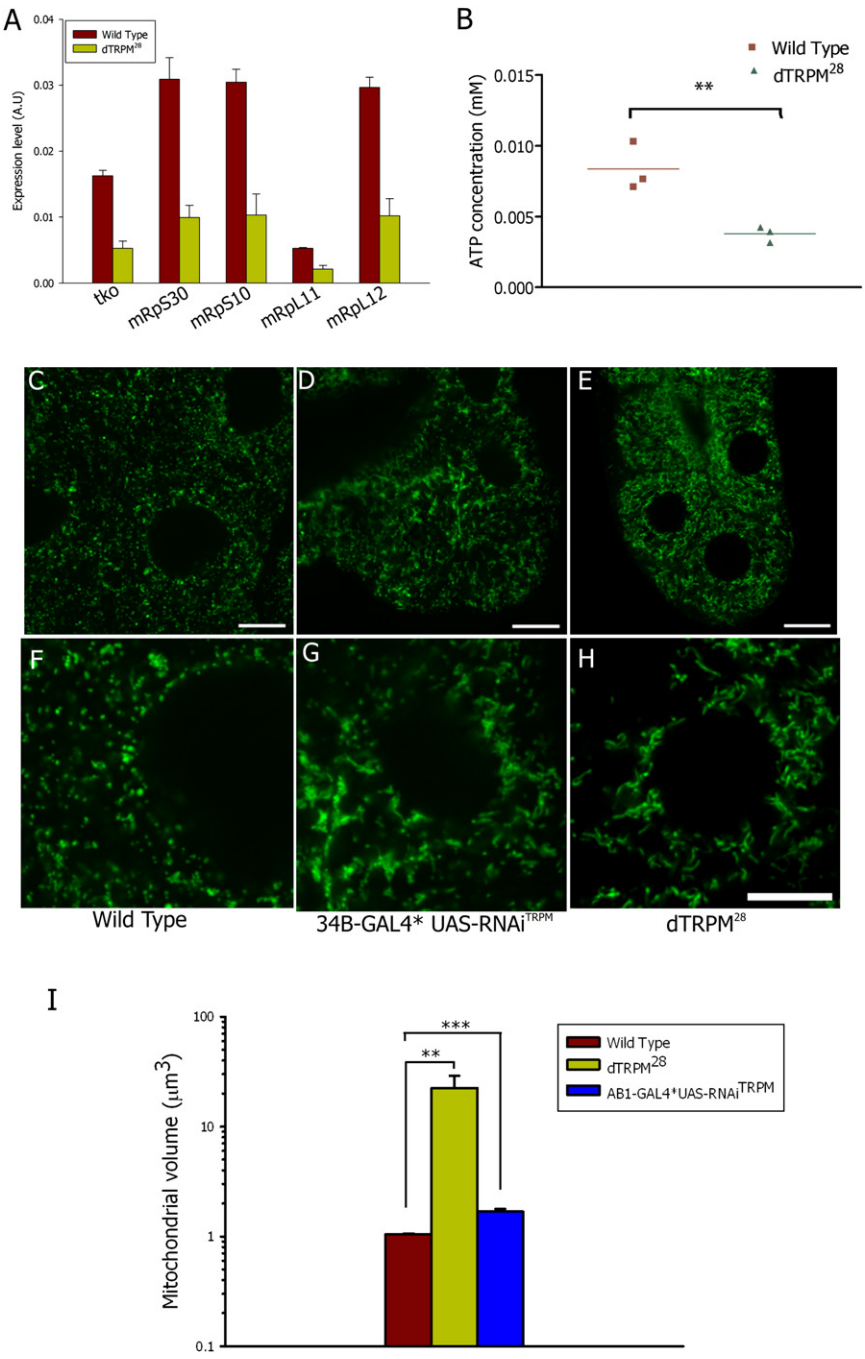

Figure 4. Altered Mitochondrial Structure and Function in *dTRPM* Mutants

(A) RT-QPCR validation of changes in transcript levels for genes encoding five individual mitoribosome genes. Transcript levels are expressed as arbitrary units (A.U.) after normalization against an endogenous control. Bars are mean ±SD (n = 3 estimations with ten larvae each).

(B) ATP levels in larval extracts from wild-type and $dTRPM^{28}$ third instar larvae. Data are shown for three separate estimations (with ten larvae each). Horizontal lines show the mean, and each symbol represents the value from an independent experiment.

(C–H) *dTRPM* loss of function leads to cell-autonomous defects in mitochondrial structure. The mitochondria are marked using a mitoGFP transgene (described in the Supplemental Experimental Procedures). Whereas wild-type salivary gland cells have a homogeneous population of small mitochondria with the classical bullet shape structure (C and F, n = 7 glands), mitochondria in $dTRPM^{28}$ salivary gland cells form long tubular structures (E and H, n = 5 glands). $RNAi^{TRPM}$ glands show an intermediate mitochondrial defect (D and G, n = 4 glands).

(I) The average volume of individual mitochondria calculated from analysis of image stacks using Volocity image analysis software is shown. Values represented are mean ±SEM. Scale bars in (C)–(E), 20 μm; in (F)–(H), 5 μm.

seen in $RNAi^{TRPM}$ glands (Figures 4D and 4G). To test the extent to which reduced mitochondrial function can explain the growth defect of $dTRPM^{28}$, we examined the effect of rotenone, a specific inhibitor of electron transfer from the iron-sulfur centers in complex I to ubiquinone on wild-type larvae. We found that wild-type larvae grown on rotenone-containing food showed a larval period lasting 48 hr longer than mock-fed controls. During larval stages, rotenone-fed animals were always lower in weight compared to wild-type controls (data not shown). These findings show that pharmacological block in mitochondrial function can recapitulate the cell growth defect in $dTRPM^{28}$.

Zn^{2+} Homeostasis Is Altered in $dTRPM^{28}$

We studied Zn^{2+} homeostasis in $dTRPM^{28}$ larvae. Using inductively coupled plasma optical emission spectrometry (ICP-OES), we found that Zn levels in wpp tissues were ca. 50% lower in $dTRPM^{28}$ compared to wild-type (Figure 5A), whereas Mg and Ca levels were not reduced (Figure 5A). In order to estimate cytoplasmic Zn^{2+} load, we used a biosensor system based on the transcription of metallothionein (*Mtn*) genes, which encode small cysteine-rich proteins that bind heavy metal ions such as Zn^{2+}, Cu^{2+}, and Cd^{2+} (Kagi, 1991, and Figure 5B). In both *Drosophila* and mammals, transcription of *Mtn* genes is regulated by trace metal load via the metal responsive transcription factor MTF (Egli et al., 2003). We used levels of *MtnC* transcripts as a readout of cytoplasmic Zn^{2+} load. RT-QPCR showed that the *MtnC* transcripts were lower in $dTRPM^{28}$ compared to wild-type throughout larval development with an increasing difference in *MtnC* transcript levels between wild-type and $dTRPM^{28}$ as development proceeds (Figure 5C).

MtnC transcription was also measured in response to Zn^{2+} feeding in third instar larvae. When wild-type larvae are fed 5 mM Zn^{2+}, *MtnC* transcripts are induced within an hour of feeding and rise progressively over the next 5 hr relative to

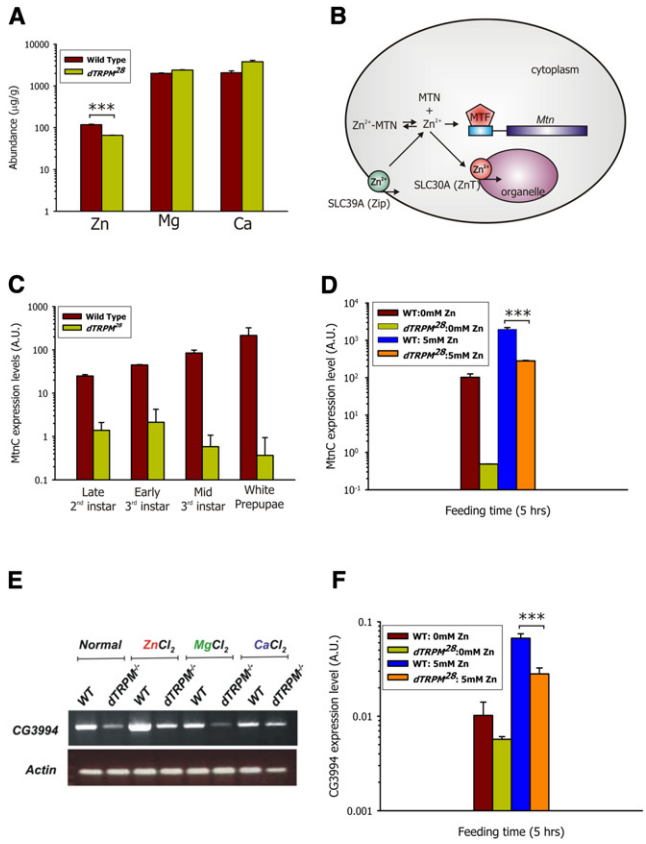

Figure 5. Altered Zn Homeostasis in *dTRPM* Mutants

(A) ICP-OES estimates of Zn, Mg, and Ca levels in larval tissue extracts from wild-type and *dTRPM*^{28}. Values are expressed as parts per million (ppm, i.e., ng/mg dry weight). Bars represent the mean of three independent estimations ±SEM for each element. Zn abundance in *dTRPM*^{28} is 56% of wild-type controls (***$p < 0.001$).

(B) Cartoon of a cell depicting key elements of the Zn^{2+} regulatory system in eukaryotes. The cytoplasm and a Zn^{2+} containing intracellular organelle are shown. Two classes of Zn^{2+} transporters SLC30A and SLC39A are shown. The binding reaction of Zn^{2+} to cytoplasmic metallothionein proteins (MTN) is shown. Zn^{2+} can also bind to the metal-dependent transcription factor (MTF) that binds to the upstream regulatory elements (blue box) of *Mtn* genes.

(C) RT-QPCR analysis of changes in *MtnC* transcripts in *dTRPM*^{28} tissues during four stages of larval development. There is both a drop in *MtnC* transcripts in *dTRPM*^{28} as well as a rise in wild-type as development proceeds. Values for transcript levels are expressed as arbitrary units (A.U.) after normalization to an endogenous control. y axis is on a log scale. Bar sizes are mean ±SD n = 3 repeats with ten larvae each.

(D) Changes in levels of *MtnC* transcripts in larval tissues in response to Zn^{2+} feeding. RT-QPCR analysis of RNA from third instar larvae maintained on plates containing 5 mM $ZnCl_2$ for 5 hr. On Zn^{2+} feeding *MtnC* transcripts are induced in both genotypes but to a lower level in *dTRPM*^{28}. Transcript levels are expressed as arbitrary units (A.U.) after normalization against an endogenous control. y axis is on a log scale. Transcript levels are show for wild-type and *dTRPM*^{28} both when feeding of nominally Zn^{2+}-free food (0 mM Zn^{2+}) and Zn^{2+}-supplemented food (5 mM Zn^{2+}). Bars are the mean ±SD n = 3 repeats with ten larvae each (***$p < 0.001$).

(E) RT-PCR analysis of the transcriptional induction of the SLC30A family Zn^{2+} transporter CG3994. Wild-type third instar larvae feeding on agar plates containing 5 mM $ZnCl_2$, $MgCl_2$, or $CaCl_2$ were analyzed. Transcripts of actin are used as a control.

(F) RT-QPCR analysis of CG3994 transcripts from larval tissues in response to Zn^{2+} feeding. Third instar larvae maintained on food containing 5 mM $ZnCl_2$ for 5 hr were analyzed. Transcript levels are expressed as arbitrary units (A.U.) after normalization against an endogenous control. y axis is on a log scale. Transcript levels are shown for wild-type and *dTRPM*^{28} both when feeding on nominally Zn^{2+}-free food (0 mM Zn^{2+}) and Zn^{2+}-supplemented food (5 mM Zn^{2+}). Bars are the mean ±SD (***$p < 0.001$).

mock-fed animals (Figure 5D). Strikingly, Zn^{2+} feeding also induced *MtnC* transcription in *dTRPM*^{28} larvae (Figure 5D), although at any given time point the levels of *MtnC* transcript in *dTRPM*^{28} larvae grown on Zn^{2+} were always lower than that in wild-type (Figure 5D).

Transporters of the SLC30A (ZnT) and SLC39A (ZiP) family are key components of the Zn^{2+} regulatory system in eukaryotes (Eide, 2006, and Figure 5B). We studied CG3994 (Yepiskoposyan et al., 2006) that encodes a member of the SLC30A family and is expected to remove Zn^{2+} from the cytoplasm (Eide, 2006). Transcription of CG3994 in wild-type *Drosophila* larvae is induced when feeding on 5 mM $ZnCl_2$ but not $MgCl_2$ or $CaCl_2$, suggesting that CG3994 transcription is specifically regulated by Zn^{2+}(Figure 5E). RT-QPCR analysis showed that CG3994 transcripts were 2.45-fold lower in *dTRPM*^{28} compared to wild-type wpp. Importantly, when *dTRPM*^{28} larvae are grown on 5 mM Zn^{2+}, the induction in CG3994 transcripts was lower than in wild-type under equivalent conditions (Figure 5F). Together, these findings strongly suggest that levels of intracellular Zn^{2+} in *dTRPM*^{28} larvae are lower than in wild-type.

Zn^{2+} Depletion Recapitulates Key Aspects of the *dTRPM*^{28} Phenotype

To test if altered Zn^{2+} homeostasis plays a role in the larval growth phenotypes seen in *dTRPM*^{28}, we used the Zn^{2+} chelator N,N,N′,N′-Tetrakis-(2-pyridylmethyl)-ethylenediamine (TPEN). TPEN is a heavy metal chelator whose affinity for Ca^{2+} and Mg^{2+} is more than ten orders of magnitude lower than that for Zn^{2+} (Anderegg and Wenk, 1967; Arslan et al., 1985). We grew wild-type larvae on food (that normally contains 50 μM Zn^{2+}) supplemented with 100 μM TPEN; at this concentration, given the K_d of TPEN for Ca^{2+} and Mg^{2+}, the levels of levels of Ca^{2+} and Mg^{2+} (normally 5.22 and 7.2 mM, respectively, in fly food) are not expected to change. When wild-type larvae are grown on food containing 100 μM TPEN, levels of the Zn^{2+}-sensitive transcript *MtnC* are massively reduced (Figure 6E), and those for the Zn^{2+} transporter CG3994 are also downregulated (Figure 6F) similar to that seen in *dTRPM*^{28}. Wild-type larvae grown on TPEN recapitulated three key aspects of the *dTRPM*^{28} phenotype. (1) The first is a dose-dependent reduction in larval weight. At 48 hr posthatching, wild-type larvae on food containing 100 μM TPEN were only 5% of the weight of those on normal food (data not shown), whereas larvae grown on 50 μM TPEN showed a smaller but substantial reduction in body weight (Figure 6A). (2) Second is a dose-dependent reduction in the average salivary gland cell size (Figure 6B). At 100 μM TPEN, average cell size in wild-type larvae was comparable to that of *dTRPM*^{28} grown on normal food (Figure 6B). Interestingly, the reduction in cell size caused by 100 μM TPEN in wild-type salivary glands was much bigger than in RNAi^{TRPM} or *dTRPM*^{28} (Figure 6C). (3) The average mitochondrial volume in salivary glands of wild-type animals grown on 50 μM TPEN was comparable to that in

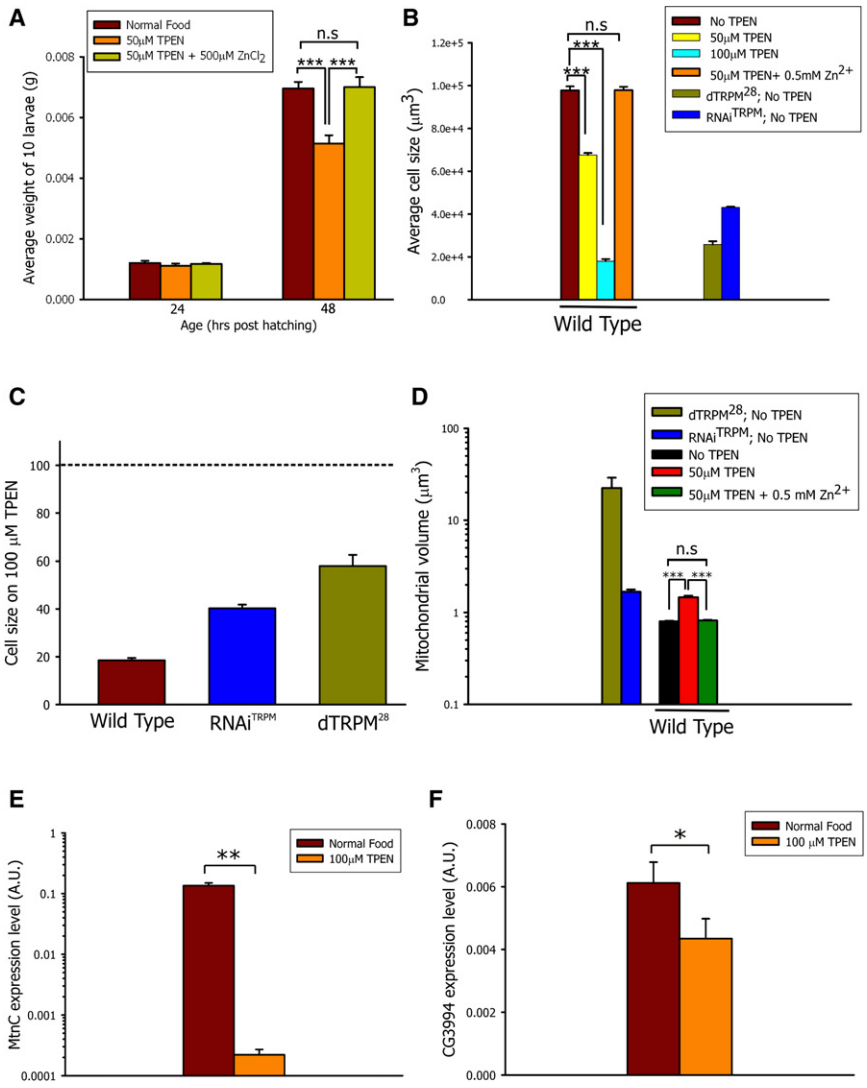

Figure 6. Zn^{2+} Depletion Phenocopies *dTRPM* Deficiency

(A) Larvae feeding on 50 μM TPEN show a reduction in body weight. Measurements are shown for animals that are 24 and 48 hr posthatching. Weight of animals grown on normal food, food supplemented with 50 μM TPEN as well as 50 μM TPEN + 0.5 mM $ZnCl_2$, are shown. y axis shows the average weight of 10 larvae. Bars represent mean ±SD n = 200 for 24 hr time point and n = 100 for 48 hr time point.

(B) Quantification of cell size changes in wild-type animals grown on normal food, TPEN (50 and 100 μM) and food containing 50 μM TPEN + 0.5 mM $ZnCl_2$. y axis shows the average size of salivary gland cells from third instar larvae. Bars represent mean ±SEM (*** indicates $p < 0.001$; n.s., not significant). Data shown represent the analysis of glands from at least four animals. Average cell size in *dTRPM*^{28} and RNAi^{TRPM} glands on normal food is shown for comparison.

(C) Effectiveness of 100 μM TPEN in reducing salivary gland cell size. y axis depicts the cell size in animals fed on TPEN relative to mock fed controls. The cell size in mock-fed animals is indicated by the dotted line. Wild-type larvae show a large reduction in cell size on TPEN in comparison to those grown on normal food, while the reduction was much smaller in RNAi^{TRPM} and *dTRPM*^{28}. Bars represent mean ±SEM.

(D) Average volume of individual mitochondria from salivary glands of wild-type third instar larvae grown on different kinds of food to manipulate Zn^{2+} availability. Bars represent the mean ±SEM (*** indicates $p < 0.001$; n.s., not significant). Data from *dTRPM*^{28} and RNAi^{TRPM} glands on normal food are shown for comparison.

(E) Comparison of *MtnC* transcript levels in extracts from larvae grown on either normal or food containing 100 μM TPEN. y axis is on a log scale. n = 3 independent experiments.

(F) Comparison of CG3994 transcript levels in extracts from larvae grown on either normal or food containing 100 μM TPEN. Transcript levels in (E) and (F) are expressed as arbitrary units (A.U.) after normalization against an endogenous control.

RNAi^{TRPM} (Figure 6D). Importantly, all three phenotypes could be suppressed by adding 0.5 mM Zn^{2+} along with 50 μM TPEN so that the added TPEN was saturated with Zn^{2+} and free Zn^{2+} was now once again available in the food (Figures 6A, 6B, and 6D). Taken together, these observations offer strong evidence that phenotypes of *dTRPM* deficiency can be recapitulated by Zn^{2+} depletion.

Extracellular Zn^{2+} Supplementation Rescues Key *dTRPM* Phenotypes

To test the role of Zn^{2+} deficiency in the cell growth defect of salivary glands lacking *dTRPM*, we grew RNAi^{TRPM} animals on food supplemented with Zn^{2+}. Analysis of cell size revealed that the addition of Zn^{2+} resulted in a rescue of salivary gland size in third instar RNAi^{TRPM} larvae (Figures 7A–7C). Quantitative analysis showed that the rescue in the cell by Zn^{2+} in RNAi^{TRPM} was dose dependent (Figures 7D–7G); rearing RNAi^{TRPM} on 20 μM Zn^{2+} resulted in a partial rescue of the cell size defect while 100 μM Zn^{2+} supplementation resulted in an average cell size that was almost wild-type (Figure 7G). Finally, imaging of mitochondrial morphology showed that the tubular nature of the mitochondria in RNAi^{TRPM} (Figures 7E and 7H) was reverted to wild-type morphology (Figures 7D and 7H) in animals grown on 100 μM Zn^{2+} (Figures 7F and 7H). These observations demonstrate that two key phenotypes of *dTRPM*-deficient salivary glands can be rescued by extracellular Zn^{2+} supplementation.

DISCUSSION

In this study, we found that functional expression of the single *dTRPM* gene generates a conductance that is suppressed by high intracellular Mg^{2+} and is permeable to a range of divalent

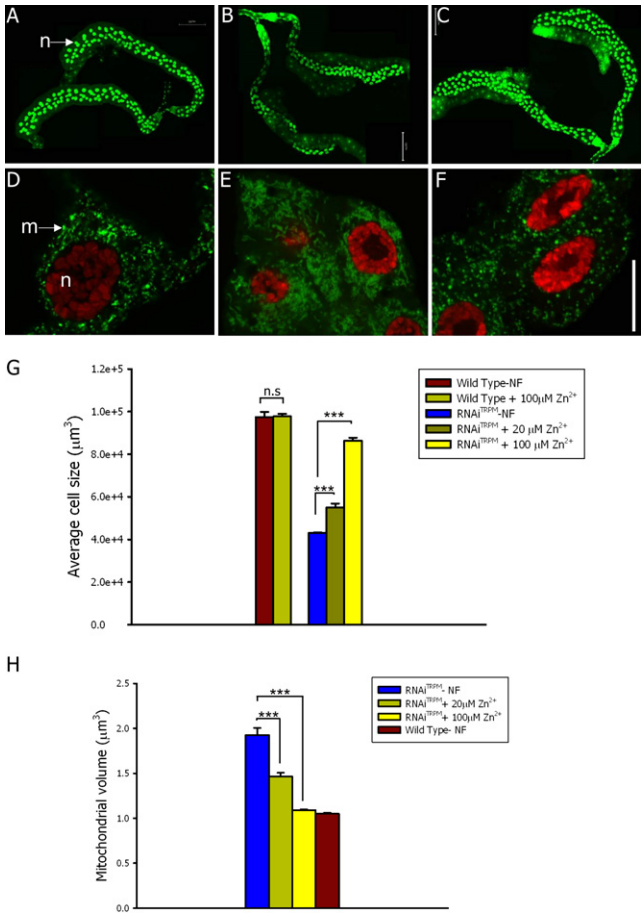

Figure 7. Rescue of dTRPM Cellular Phenotypes by Zn^{2+} Supplementation

(A–C) Maximum projection montages of a series of overlapping image stacks from salivary glands of wild-type (A) glands where *dTRPM* has been depleted by RNAi ($RNAi^{TRPM}$) (B) and $RNAi^{TRPM}$ glands from animals grown on food which has been supplemented with 100 μM Zn^{2+}(C). The nuclei of individual salivary glands cells are shown stained with the nuclear dye TOTO-3 and marked n.

(D–F) High-magnification images of cells from individual salivary gland cells of wild-type (D) $RNAi^{TRPM}$ glands (E) and $RNAi^{TRPM}$ glands on 100 μM Zn^{2+}-supplemented food (F). The nucleus is marked n stained with TOTO-3, and mitochondria are marked m and detected using a mitoGFP transgene.

(G) Quantitative analysis of the effect of Zn^{2+} supplementation on the cell size of *dTRPM*-deficient salivary glands. y axis indicates the average cell size. Bars represent the mean ±SEM. Data are derived from glands taken from at least four different animals. *** indicates $p < 0.001$; n.s. indicates not significant. The average cell size from $dTRPM^{28}$ and $RNAi^{TRPM}$ glands is shown for comparison.

(H) Quantitative analysis of the effect of Zn^{2+} supplementation on the mitochondrial morphology in *dTRPM*-deficient cells. y axis indicates the average size of individual mitochondria from salivary gland cells of third instar larvae. Bars represent mean ±SEM. *** indicates $p < 0.001$.

cations. This divalent permeability was abolished in a pore mutant (E1007Q), strongly suggesting that dTRPM is part of an ion-conducting pore. While the dTRPM conductance permeates a range of divalent cations, it is especially conductive to Zn^{2+} (Figure 1F), and its permeability profile is reminiscent of that reported for mammalian TRPM6 and TRPM7 (Li et al., 2006; Monteilh-Zoller et al., 2002) and TRPM3α2 (Wagner, et al., 2010).

During this study, we made four key observations: (1) Zn^{2+} depletion in wild-type larvae can recapitulate the cell size and mitochondrial defects seen in *dTRPM*-deficient salivary glands (Figures 6B and 6D); (2) the effects of Zn^{2+} depletion on salivary gland cell size was smaller in *dTRPM*-deficient cells compared to wild-type (Figure 6C); (3) the defects in cell size and mitochondrial morphology of *dTRPM*-deficient cells could be rescued by supplementation with extracellular Zn^{2+} (Figure 7); (4) finally, $dTRPM^{28}$ larvae show defects in Zn^{2+} homeostasis (Figure 5). These observations strongly suggest a causal relationship between altered Zn^{2+} homeostasis and the cellular phenotypes of *dTRPM* deficiency in vivo. Taken together, they provide compelling evidence of a role for dTRPM-dependent Zn^{2+} homeostasis in supporting cell growth during *Drosophila* larval development. Consistent with our findings of altered Zn^{2+} homeostasis and associated larval growth defect in $dTRPM^{28}$, embryonic growth defects have been reported in a mouse KO of the SLC30A family Zn^{2+} transporter ZnT1 (Andrews et al., 2004), and RNAi knockdown of the *Drosophila* ortholog of ZnT1, required for Zn^{2+} uptake in intestinal cells, results in growth defects during larval development (Wang et al., 2009). Interestingly, although a number of previous studies have implicated Mg^{2+} permeation through mammalian TRPM7 as relevant for its physiological function (Sahni and Scharenberg, 2008; Schmitz et al., 2003), a recent study has reported that Mg^{2+} levels and homeostasis are unaffected in TRPM7 K/O mice (Jin et al., 2008). Like dTRPM, TRPM7 has also been reported to be particularly permeable to Zn^{2+} (Li et al., 2006; Monteilh-Zoller et al., 2002); thus it will be interesting to study if Zn^{2+} homeostasis in mammalian systems is regulated by TRPM7.

What is the role of dTRPM in regulating cellular Zn^{2+}? Our results demonstrate Zn^{2+} induced *MtnC* transcription following extracellular Zn^{2+} supplementation in $dTRPM^{28}$ cells (Figure 5D), implying Zn^{2+} entry into the cytoplasm. This result suggests that dTRPM is unlikely to be the exclusive or major route of Zn^{2+} influx across the plasma membrane; rather, the major route of Zn^{2+} entry across the plasma membrane is dependent on Zn^{2+} transporters. It is more likely that dTRPM regulates Zn^{2+} homeostasis in a specific subcellular compartment that plays a critical, nonredundant role in growth. Presently the subcellular localization of endogenous dTRPM channels is unknown; this information will be critical to defining the subcellular compartment in which dTRPM regulates Zn^{2+} homeostasis. Whatever the nature of this compartment, it is likely that there will be complex but important crosstalk between dTRPM and Zn^{2+} transporters. Our observation of altered CG3994 transcription in $dTRPM^{28}$ is an indication of this (Figure 5F). Further analysis of the interactions between dTRPM with Zn^{2+} transporters with respect to cell size regulation will be required to unravel the nature of this crosstalk.

The rapid and dramatic increase in body mass during *Drosophila* larval development is almost entirely underpinned by increases in cell size in larval-specific tissues (Church and Robertson, 1966). Although a complex neuroendocrine axis coordinates this growth (reviewed in Edgar, 2006; Mirth and Riddiford, 2007), in this study we found that the requirement of *dTRPM* to support salivary gland cell growth was cell

autonomous. This requirement for dTRPM function in cell growth appears to be subsequent to normal activation of class I PI3K and its key downstream growth regulator S6K (Figure 3) and independent of altered dFOXO function (detailed in Figure S5). These data offer compelling evidence of a requirement for dTRPM function for molecular processes that operate subsequent to activation of dS6K. Interestingly, DT-40 chicken B-lymphoma cell lines with TRPM7 deleted have been reported to have a small reduction in cell size (Sahni and Scharenberg, 2008), although the proposed function of TRPM7 in this setting is mechanistically different.

Since our data indicate a strong causal relationship between altered Zn^{2+} homeostasis and cell growth in *dTRPM*^{28} that occurs downstream of S6K activation, what molecular processes might be affected? The *Drosophila* genome contains ca. 500 proteins with obvious Zn^{2+}-binding motifs (such as Zn^{2+} fingers), and it is very likely that multiple Zn^{2+}-dependent molecular processes are affected by the loss of *dTRPM*. However, given that the incorporation of new biomass is a key element of increase in cell size, it is likely that Zn^{2+}-dependent processes that affect macromolecular biosynthesis are impaired. In most cells, protein synthesis consumes more energy than any other biosynthetic process; at least four high-energy phosphate bonds are split to make each new peptide bond. We found defects in mitochondrial structure and function in dTRPM-deficient cells (Figure 4) that could be recapitulated in wild-type larvae by Zn^{2+} depletion (Figure 6) and suppressed in dTRPM-deficient salivary gland cells by extracellular Zn^{2+} supplementation (Figure 7). Taken together, these observations imply an important role for dTRPM-dependent Zn^{2+} homeostasis in regulating mitochondrial structure in *Drosophila* salivary gland cells. Along with similar larval growth phenotypes reported for mutants in genes encoding mitochondrial ribosomes (Frei et al., 2005; Toivonen et al., 2001; Tselykh et al., 2005), the altered mitochondrial structure and the reduced ATP levels in *dTRPM*^{28} that we report (Figure 4) strongly suggest that the cellular growth defect in *dTRPM*^{28} larvae is underpinned by a major deficit in cellular energy supply required to undertake protein biosynthesis. However, this does not preclude additional roles for other Zn^{2+}-dependent cellular processes (such as the function of transcription factors, chromatin remodeling enzymes, and other proteins) in the cell growth defect seen in *dTRPM* mutants.

EXPERIMENTAL PROCEDURES

RNA Extraction and QPCR

Total RNA was extracted from various fly tissues and developmental stages using TRIzol reagent (Invitrogen). Purified RNA was treated with Amplification grade DNase I (Invitrogen). SuperScript II RNase H^- Reverse Transcriptase (Invitrogen) and RNase H (Roche) treatments were carried out subsequently.

RT-QPCR was performed using Taqman Gene Expression Assays (Applied Biosystems). Transcript levels of the ribosomal protein RP49 were used for normalization across samples. Three separate samples were collected from each genotype, and duplicate measures of each sample were conducted to ensure the consistency of the amplification.

Cloning and Sequencing *dTRPM*

EXL DNA Polymerase(Stratagene) was used for PCR amplification of a 5847 bp fragment which includes the entire *dTRPM* ORF using gene-specific primers. The PCR product was gel purified and cloned into pCR-XL-TOPO vector (Invitrogen) followed by sequencing (Cogenics Lark UK).

Electrophysiology

Standard whole-cell patch-clamp experiments were performed on HEK293 cells as described previously (Wagner et al., 2008). Current traces were obtained by offline analysis from voltage ramps applied at a rate of one per second. The composition of the solution and a more detailed description of the procedures are given in the Supplemental Experimental Procedures section.

ICP-OES Analysis

Wpp were collected in 1.5 ml Eppendorf tubes (10 wpp/tube) and their wet weight measured. They were then oven dried at 70°C–75°C for 7 days and dissolved in 65% HNO_3 (TraceSELECT Ultra, Fluka [Sigma 02650]) for 7 days at room temperature. Following this, H_2O_2 (TraceSELECT Ultra, Fluka [Sigma 16911]) was added and digested for a further 7 days. Samples were diluted with ultrapure water (18.2 MΩ), centrifuged at 20,000 g for 10 min, and the supernatant subjected to ICP-OES analysis. ICP-OES analysis for Zn, Mg, and Ca was performed by Warwick Analytical Services Ltd (UK) on a Perkin Elmer 5300DV instrument using a four point calibration in the range 0–100 ppB for each element. Spectral emissions for each metal were measured at two independent wavelengths.

Immunocytochemistry

Tissues dissected from late third instar larvae or wpp were fixed in 4% formaldehyde in PBS for 20 min. Samples were then incubated overnight at 4°C in the primary antibody, followed by an appropriate fluorescently conjugated secondary antibody for 2 hr at room temperature. Where required, nuclei were counterstained using the TOTO3 nuclear stain (Molecular Probes, T-3604). Individual tissues were mounted in Vectashield for confocal imaging.

Imaging

All images were acquired on a Zeiss 510LSM Meta point-scanning confocal microscope, using a 20× (Plan neofluor, N.A:0.50) or a 40× oil objective (Plan neofluar, N.A: 1.30). 3D images of whole salivary glands were generated by acquiring a series of overlapping image stacks. Using Volocity image analysis software, we measured the total volume of the gland, as well as the number of nuclei, leading to an estimate of the average cell size. A total of at least four salivary glands from different animals were analyzed per genotype.

Further detailed materials and methods are available in the Supplemental Experimental Procedures.

SUPPLEMENTAL INFORMATION

Supplemental Information includes five figures, one table, Supplemental Experimental Procedures, and Supplemental References and can be found with this article at doi:10.1016/j.cmet.2010.08.012.

ACKNOWLEDGMENTS

We thank S. Andrews and J. Coadwell for help with bioinformatics, A. Segonds-Pichon with help with statistical analysis, and M. Portz and S. Plant for excellent technical support. We thank numerous colleagues for providing fly stocks used in this study. P.R. acknowledges the support of J. Hughes, S. McNulty, and M. Skingle during this study. This work was funded by the UK MRC, BBSRC (R.P.), and DFG through its Emmy Noether program and by HOMFOR (J.O.).

Received: September 11, 2009
Revised: April 26, 2010
Accepted: June 24, 2010
Published: October 5, 2010

REFERENCES

Aarts, M., Iihara, K., Wei, W.L., Xiong, Z.G., Arundine, M., Cerwinski, W., MacDonald, J.F., and Tymianski, M. (2003). A key role for TRPM7 channels in anoxic neuronal death. Cell *115*, 863–877.

Anderegg, G., and Wenk, F. (1967). Pyridinderivate als Komplexbildner VIII Die Herstellung je eines neuen vier- und sechszähnigen Liganden. Helv. Chim. Acta *50*, 2330–2332.

Andrews, G.K., Wang, H., Dey, S.K., and Palmiter, R.D. (2004). Mouse zinc transporter 1 gene provides an essential function during early embryonic development. Genesis *40*, 74–81.

Arslan, P., Di Virgilio, F., Beltrame, M., Tsien, R.Y., and Pozzan, T. (1985). Cytosolic Ca2+ homeostasis in Ehrlich and Yoshida carcinomas. A new, membrane-permeant chelator of heavy metals reveals that these ascites tumor cell lines have normal cytosolic free Ca2+. J. Biol. Chem. *260*, 2719–2727.

Barcelo, H., and Stewart, M.J. (2002). Altering Drosophila S6 kinase activity is consistent with a role for S6 kinase in growth. Genesis *34*, 83–85.

Britton, J.S., Lockwood, W.K., Li, L., Cohen, S.M., and Edgar, B.A. (2002). Drosophila's insulin/PI3-kinase pathway coordinates cellular metabolism with nutritional conditions. Dev. Cell *2*, 239–249.

Cao, G., Thebault, S., van der Wijst, J., van der Kemp, A., Lasonder, E., Bindels, R.J., and Hoenderop, J.G. (2008). RACK1 inhibits TRPM6 activity via phosphorylation of the fused alpha-kinase domain. Curr. Biol. *18*, 168–176.

Church, R.B., and Robertson, F.W. (1966). Biochemical analysis of genetic differences in the growth of Drosophila. Genet. Res. *7*, 383–407.

Clark, K., Middelbeek, J., Morrice, N.A., Figdor, C.G., Lasonder, E., and van Leeuwen, F.N. (2008). Massive autophosphorylation of the Ser/Thr-rich domain controls protein kinase activity of TRPM6 and TRPM7. PLoS One *3*, e1876. 10.1371/journal.pone.0001876.

Damann, N., Voets, T., and Nilius, B. (2008). TRPs in our senses. Curr. Biol. *18*, R880–R889.

Drennan, D., and Ryazanov, A.G. (2004). Alpha-kinases: analysis of the family and comparison with conventional protein kinases. Prog. Biophys. Mol. Biol. *85*, 1–32.

Edgar, B.A. (2006). How flies get their size: genetics meets physiology. Nat. Rev. Genet. *7*, 907–916.

Egli, D., Selvaraj, A., Yepiskoposyan, H., Zhang, B., Hafen, E., Georgiev, O., and Schaffner, W. (2003). Knockout of 'metal-responsive transcription factor' MTF-1 in Drosophila by homologous recombination reveals its central role in heavy metal homeostasis. EMBO J. *22*, 100–108.

Eide, D.J. (2006). Zinc transporters and the cellular trafficking of zinc. Biochim. Biophys. Acta *1763*, 711–722.

Elizondo, M.R., Arduini, B.L., Paulsen, J., MacDonald, E.L., Sabel, J.L., Henion, P.D., Cornell, R.A., and Parichy, D.M. (2005). Defective skeletogenesis with kidney stone formation in dwarf zebrafish mutant for trpm7. Curr. Biol. *15*, 667–671.

Fleig, A., and Penner, R. (2004). The TRPM ion channel subfamily: molecular, biophysical and functional features. Trends Pharmacol. Sci. *25*, 633–639.

Frei, C., Galloni, M., Hafen, E., and Edgar, B.A. (2005). The Drosophila mitochondrial ribosomal protein mRpL12 is required for Cyclin D/Cdk4-driven growth. EMBO J. *24*, 623–634.

Jin, J., Desai, B.N., Navarro, B., Donovan, A., Andrews, N.C., and Clapham, D.E. (2008). Deletion of Trpm7 disrupts embryonic development and thymopoiesis without altering Mg2+ homeostasis. Science *322*, 756–760.

Kagi, J.H. (1991). Overview of metallothionein. Methods Enzymol. *205*, 613–626.

Kwan, C.S., Vazquez-Manrique, R.P., Ly, S., Goyal, K., and Baylis, H.A. (2008). TRPM channels are required for rhythmicity in the ultradian defecation rhythm of C. elegans. BMC Physiol. *8*, 11.

Li, M., Jiang, J., and Yue, L. (2006). Functional characterization of homo- and heteromeric channel kinases TRPM6 and TRPM7. J. Gen. Physiol. *127*, 525–537.

Li, M., Du, J., Jiang, J., Ratzan, W., Su, L.T., Runnels, L.W., and Yue, L. (2007). Molecular determinants of Mg2+ and Ca2+ permeability and pH sensitivity in TRPM6 and TRPM7. J. Biol. Chem. *282*, 25817–25830.

Ma, X.M., and Blenis, J. (2009). Molecular mechanisms of mTOR-mediated translational control. Nat. Rev. Mol. Cell Biol. *10*, 307–318.

McKemy, D.D., Neuhausser, W.M., and Julius, D. (2002). Identification of a cold receptor reveals a general role for TRP channels in thermosensation. Nature *416*, 52–58.

Mederos y Schnitzler, M., Waring, J., Gudermann, T., and Chubanov, V. (2008). Evolutionary determinants of divergent calcium selectivity of TRPM channels. FASEB J. *22*, 1540–1551.

Mirth, C.K., and Riddiford, L.M. (2007). Size assessment and growth control: how adult size is determined in insects. Bioessays *29*, 344–355.

Monteilh-Zoller, M.K., Hermosura, M.C., Nadler, M.J.S., Scharenberg, A.M., Penner, R., and Fleig, A. (2002). TRPM7 provides an ion channel mechanism for cellular entry of trace metal ions. J. Gen. Physiol. *121*, 49–60.

Montell, C. (2003). The venerable inveterate invertebrate TRP channels. Cell Calcium *33*, 409–417.

Nadler, M.J., Hermosura, M.C., Inabe, K., Perraud, A.L., Zhu, Q., Stokes, A.J., Kurosaki, T., Kinet, J.P., Penner, R., Scharenberg, A.M., et al. (2001). LTRPC7 is a Mg.ATP-regulated divalent cation channel required for cell viability. Nature *411*, 590–595.

Nilius, B., Prenen, J., Janssens, A., Owsianik, G., Wang, C., Zhu, M.X., and Voets, T. (2005). The selectivity filter of the cation channel TRPM4. J. Biol. Chem. *280*, 22899–22906.

Oberwinkler, J., Lis, A., Giehl, K.M., Flockerzi, V., and Philipp, S.E. (2005). Alternative splicing switches the divalent cation selectivity of TRPM3 channels. J. Biol. Chem. *280*, 22540–22548.

Owsianik, G., Talavera, K., Voets, T., and Nilius, B. (2006). Permeation and selectivity of TRP channels. Annu. Rev. Physiol. *68*, 685–717.

Padinjat, R., and Andrews, S. (2004). TRP channels at a glance. J. Cell Sci. *117*, 5707–5709.

Peier, A.M., Moqrich, A., Hergarden, A.C., Reeve, A.J., Andersson, D.A., Story, G.M., Earley, T.J., Dragoni, I., McIntyre, P., Bevan, S., et al. (2002). A TRP channel that senses cold stimuli and menthol. Cell *108*, 705–715.

Pel, H.J., and Grivell, L.A. (1994). Protein synthesis in mitochondria. Mol. Biol. Rep. *19*, 183–194.

Ramsey, I.S., Delling, M., and Clapham, D.E. (2006). An introduction to TRP channels. Annu. Rev. Physiol. *68*, 619–647.

Ryazanov, A.G., Ward, M.D., Mendola, C.E., Pavur, K.S., Dorovkov, M.V., Wiedmann, M., Erdjument-Bromage, H., Tempst, P., Parmer, T.G., Prostko, C.R., et al. (1997). Identification of a new class of protein kinases represented by eukaryotic elongation factor-2 kinase. Proc. Natl. Acad. Sci. USA *94*, 4884–4889.

Ryazanova, L.V., Dorovkov, M.V., Ansari, A., and Ryazanov, A.G. (2004). Characterization of the protein kinase activity of TRPM7/ChaK1, a protein kinase fused to the transient receptor potential ion channel. J. Biol. Chem. *279*, 3708–3716.

Sahni, J., and Scharenberg, A.M. (2008). TRPM7 ion channels are required for sustained phosphoinositide 3-kinase signaling in lymphocytes. Cell Metab. *8*, 84–93.

Schlingmann, K.P., Weber, S., Peters, M., Niemann Nejsum, L., Vitzthum, H., Klingel, K., Kratz, M., Haddad, E., Ristoff, E., Dinour, D., et al. (2002). Hypomagnesemia with secondary hypocalcemia is caused by mutations in TRPM6, a new member of the TRPM gene family. Nat. Genet. *31*, 166–170.

Schmitz, C., Perraud, A.L., Johnson, C.O., Inabe, K., Smith, M.K., Penner, R., Kurosaki, T., Fleig, A., and Scharenberg, A.M. (2003). Regulation of vertebrate cellular Mg2+ homeostasis by TRPM7. Cell *114*, 191–200.

Stephens, L., Anderson, K., Stokoe, D., Erdjument-Bromage, H., Painter, G.F., Holmes, A.B., Gaffney, P.R., Reese, C.B., McCormick, F., Tempst, P., et al. (1998). Protein kinase B kinases that mediate phosphatidylinositol 3,4,5-trisphosphate-dependent activation of protein kinase B. Science *279*, 710–714.

Teramoto, T., Lambie, E.J., and Iwasaki, K. (2005). Differential regulation of TRPM channels governs electrolyte homeostasis in the *C. elegans* intestine. Cell Metab. *1*, 343–354.

Toivonen, J.M., O'Dell, K.M., Petit, N., Irvine, S.C., Knight, G.K., Lehtonen, M., Longmuir, M., Luoto, K., Touraille, S., Wang, Z., et al. (2001). Technical knockout, a Drosophila model of mitochondrial deafness. Genetics *159*, 241–254.

Tselykh, T.V., Roos, C., and Heino, T.I. (2005). The mitochondrial ribosome-specific MrpL55 protein is essential in Drosophila and dynamically required during development. Exp. Cell Res. *307*, 354–366.

Voets, T., Nilius, B., Hoefs, S., van der Kemp, A.W., Droogmans, G., Bindels, R.J., and Hoenderop, J.G. (2004). TRPM6 forms the Mg2+ influx channel involved in intestinal and renal Mg2+ absorption. J. Biol. Chem. *279*, 19–25.

Wagner, T.F., Loch, S., Lambert, S., Straub, I., Mannebach, S., Mathar, I., Dufer, M., Lis, A., Flockerzi, V., Philipp, S.E., et al. (2008). Transient receptor potential M3 channels are ionotropic steroid receptors in pancreatic beta cells. Nat. Cell Biol. *10*, 1421–1430.

Wagner, T.F., Drews, A., Loch, S., Mohr, F., Philipp, S.E., Lambert, S., and Oberwinkler, J.O. (2010). TRPM3 channels provide a regulated influx pathway for zinc in pancreatic beta cells. Pflugers Arch. *460*, 755–765.

Wang, X., Wu, Y., and Zhou, B. (2009). Dietary zinc absorption is mediated by ZnT1 in Drosophila melanogaster. FASEB J. *23*, 2650–2661.

West, R.J., Sun, A.Y., Church, D.L., and Lambie, E.J. (2001). The C. elegans gon-2 gene encodes a putative TRP cation channel protein required for mitotic cell cycle progression. Gene *266*, 103–110.

Xia, R., Mei, Z.Z., Mao, H.J., Yang, W., Dong, L., Bradley, H., Beech, D.J., and Jiang, L.H. (2008). Identification of pore residues engaged in determining divalent cationic permeation in transient receptor potential melastatin subtype channel 2. J. Biol. Chem. *283*, 27426–27432.

Xiao, R., and Xu, X.Z. (2009). Function and regulation of TRP family channels in C. elegans. Pflugers Arch. *458*, 851–860.

Yepiskoposyan, H., Egli, D., Fergestad, T., Selvaraj, A., Treiber, C., Multhaup, G., Georgiev, O., and Schaffner, W. (2006). Transcriptome response to heavy metal stress in Drosophila reveals a new zinc transporter that confers resistance to zinc. Nucleic Acids Res. *34*, 4866–4877.

Zhang, Y., Hoon, M.A., Chandrashekar, J., Mueller, K.L., Cook, B., Wu, D., Zuker, C.S., and Ryba, N.J. (2003). Coding of sweet, bitter, and umami tastes: different receptor cells sharing similar signaling pathways. Cell *112*, 293–301.